

X-ray properties of 4U 1543–624

J. Schultz*

Observatory, P. O. Box 14, FIN-00014 University of Helsinki, Finland

Received / Accepted

Abstract. 4U 1543–624 is a relatively bright persistent low-mass X-ray binary. Analysis of archival data from ASCA, SAX and RXTE is presented. The X-ray continuum can be modeled with the standard low-mass X-ray binary spectrum, an isothermal blackbody and a Comptonized component. Variations in the luminosity and flux ratio of the continuum components are seen. An increase in luminosity is accompanied by a decrease in the blackbody luminosity and a hardening of the spectrum. Most low-mass X-ray binaries have softer spectra and higher blackbody luminosities in high luminosity states. The Fe K_{α} line is seen only in the high luminosity spectra. A narrow feature near 0.7 keV, previously detected in the ASCA data, is also seen in the SAX data. A qualitative model of the system is presented. The X-ray observations can be explained by a low inclination system (face-on disk) containing a slowly ($P \gg$ ms) rotating neutron star. A slowly rotating neutron star would imply either that the system is a young low-mass X-ray binary, or that the accretion rate is unusually low. The empirical relation between optical and X-ray luminosity and orbital period suggests a relatively short period.

Key words. binaries:close – stars:individual (4U 1543–624) – X-rays:binaries

1. Introduction

In low-mass X-ray binaries (LMXB) a stellar-mass black hole or neutron star accretes from a low-mass companion star. X-ray emission powered by the accretion flow dominates the bolometric luminosity in LMXBs. Detailed studies of LMXBs may be helpful in understanding the physics of accretion and compact objects, as well as the evolution of close binary stars.

4U 1543–624 is a relatively bright LMXB discovered by UHURU. It has been observed at roughly constant flux levels by most major X-ray satellites over the last decades (Singh et al. 1994; Christian & Swank 1997; Asai et al. 2000; Juett et al. 2001). The optical counterpart has been identified as a faint ($B \approx 20$) star (McClintock et al. 1978). (For a finding chart, see also Apparao et al. (1978)). Spectral analysis of EXOSAT data shows that the X-ray continuum can be modeled with an isothermal blackbody (BB) and a Comptonized component (Singh et al. 1994), a model that fits most LMXB spectra quite well (White et al. 1988). Narrow spectral features have also been detected: the Fe K_{α} line at $\simeq 6.5$ keV (Singh et al. 1994; Gottwald et al. 1995; Asai et al. 2000) and a feature at $\simeq 0.7$ keV, which may be an emission line or an artifact caused by enhanced Ne absorption (Juett et al. 2001). In this paper, archival SAX, ASCA and RXTE observations of 4U 1543–624 are ana-

Table 1. List of pointed observations used for detailed spectral analysis. Exposure times are in kiloseconds.

Satellite	Date	Instrument	Exposure
ASCA	17/8/1995	GIS	12
		SIS	10
SAX	21/2/1997	LECS	7
		MECS	18
SAX	1/4/1997	LECS	5
		MECS	18
XTE	5/5/1997	PCA	3
XTE	6/5/1997	PCA	8
XTE	7/5/1997	PCA	6
XTE	12/5/1997	PCA	7
XTE	14/5/1997	PCA	3
XTE	22/9/1997	PCA	5
XTE	13/10/1997	PCA	5

lyzed. Results of temporal and spectral variability analysis are discussed.

2. Observations and data reductions

Observations made with the narrow-field instruments of SAX, i.e. LECS (Parmar et al. 1997), MECS (Boella et al. 1997), HPGSPC (Manzo et al. 1997) and PDS (Frontera et al. 1997), all three RXTE (Bradt et al. 1993) instruments, i.e. HEXTE, PCA (Jahoda et al. 1996) and ASM (Levine et al. 1996), and both ASCA (Tanaka et al. 1994) instruments, i.e. GIS

* Juho.Schultz@astro.helsinki.fi

and SIS are analyzed. Of these, LECS, MECS, PCA, GIS and SIS (See Table 1) had data with sufficient S/N for spectral analysis.

The event lists provided by on-line archives were used for both SAX and ASCA data. Raw RXTE data were used for both PCA (‘Good Xenon’ or ‘Standard 2’-modes) and HEXTE analysis. The ‘definitive’ RXTE ASM data were used to study the long-term variability of 4U 1543–624.

2.1. SAX

For the SAX data, cleaned event lists were downloaded from the ASDC website. The LECS and MECS spectra were extracted from a 4’ region at the center of the field-of-view. The standard response files provided by ASDC were used. The background spectra were extracted from the blank-sky event lists available at ASDC using the same extraction regions as for the source spectra. The PDS and HPGSPC spectra were background-dominated, and not used for further analysis.

2.2. ASCA

The standard filtering criteria were used to produce a cleaned event list from the raw event list. The GIS2 count rate was ~ 16 cps, so significant pileup is expected in the SIS data. As the SIS data was in single-frame mode, the spectrum could be extracted with the `corpileup` tool. For SIS, the background spectrum was extracted from a blank-sky event list. The background was compared to a spectrum extracted from the science data from a region without sources at the same off-axis distance as the source. The difference between alternative background models was small, and as the SIS data is affected by pileup and the background flux is less than 0.5 % of the source flux, instrumental effects probably dominate the uncertainties of the data. For GIS, a blank-sky event list was used for background extraction. The extraction radii used were 6’ for GIS and 4’ for SIS. The response files were generated by the techniques recommended in the ASCA Data Reduction Guide¹. To improve the signal-to-noise ratio, the separate data and calibration files of the two GIS and two SIS detectors were combined into files containing all GIS data and all SIS data.

2.3. RXTE

PCA and HEXTE target and background spectra and lightcurves were extracted from the raw data. The PCA data was also used to create response files and power spectra. The data were processed as recommended in the RXTE Users’ Guide² to get cleaned event lists. For HEXTE, the responses available at the HEXTE calibration status website³, were used. Fitting a powerlaw to the

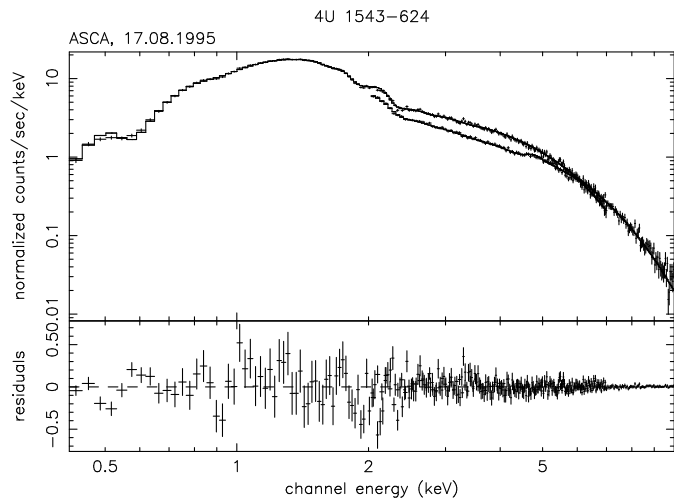


Fig. 1. The ASCA data (SIS and GIS), a fitted spectral model with blackbody and Comptonized components, and line emission at 0.676 keV. The lower panel shows the residuals.

summed HEXTE spectra (between 15–200 keV) gives a 3σ upper limit of $1.4 \cdot 10^{-13} \text{ Wm}^{-2}$ for the high-energy flux (15–200 keV band). No further spectral analysis of the HEXTE data was made.

2.4. Spectral fitting

The XSPEC v. 11.0 spectral fitting package (Arnaud 1996) was used for spectral analysis. The data used for fitting were in the 0.14–4 keV band for LECS, 1.8–10 keV for MECS, 0.4–7 keV for SIS, 1.0–10 keV for GIS and 3–20 keV for PCA.

To avoid possible instrument inter-calibration problems in the cases of ASCA (GIS/SIS) and SAX (MECS/LECS), a constant multiplier for one of the instruments was included in the fits. For ASCA, the difference in flux between GIS and SIS was $2.7 \pm 0.8\%$. In the SAX data, the MECS/LECS ratio was 0.70 ± 0.01 for the final spectral model. The ratio should be in the range 0.7–1.0 (Fiore et al. 1999), so the result is on the edge of the allowed range.

A systematic error of 1 % is usually added to the PCA data for spectral fitting. This was not applied, as the best models have $\chi_\nu \simeq 1$ even without systematic errors. To justify the inclusion of additional spectral components, the $\Delta\chi^2$ was also calculated with systematic errors of 1 % and 2 %. During the fits to PCA data, the column density of interstellar matter was held fixed to the weighted mean of the values derived from ASCA and SAX fits, $N_{\text{H}} = 33.0 \pm 3.5 \cdot 10^{24} \text{ m}^{-2}$. As no PCA data below 3 keV was used in the analysis, column depths of this order should have only minor effects. To justify the fixed column depth, fits with a freely varying column depth were made to the PCA spectra. The column densities tended to diverge toward zero. Upper limits for the N_{H} could not always be derived. When the limits could be derived, typ-

¹ <http://heasarc.gsfc.nasa.gov/docs/asca/abc/abc.html>

² <http://heasarc.gsfc.nasa.gov/docs/xte/abc/contents.html>

³ http://mamaccass.ucsd.edu:8080/hexte/hexte_calib.html

ical 3σ upper limits were of the order $1 - 3 \cdot 10^{26} \text{ m}^{-2}$. The other spectral parameters were nearly identical, but their error ranges increased by about 20 %. The spectral fits to PCA data give flux estimates of the order $3 \cdot 10^{-14} \text{ W m}^{-2}$ for the flux above 15 keV, which is consistent with the HEXTE data.

Several single component spectral models (isothermal and multicolor blackbody (Makishima et al. 1986), thermal bremsstrahlung, powerlaw, cut-off powerlaw and some Comptonization models) were tried, all with photoelectric absorption from the ISM. No single component model gave an acceptable fit, with typical values of $\chi^2_\nu > 2.5$. Two-component spectra with an isothermal blackbody (BB) as one component and a cut-off powerlaw or one of the Comptonization models, CompST (Sunyaev & Titarchuk 1980) or CompTT (Titarchuk 1994), as the other component gave the best fits. The BB-CompST fit was in most cases the best. In three cases, CompTT or powerlaw gave a better fit than CompST, but the differences were not statistically significant. The improvement in χ^2_ν was less than 0.01. The high optical depths of the Comptonization fits mean that the fitted spectra are relatively close to a cut-off powerlaw. In two cases, a combination of a multicolor blackbody and a powerlaw also gave a statistically acceptable fit. The CompST model was adopted for further analysis, as this would allow a meaningful comparison between the spectra of different observations.

The continuum fits were further improved by adding gaussian features when the residuals of the fits seemed to have a line component. In the SAX and ASCA data, a gaussian feature was detected near 0.67 keV. The Fe K_α line could not be detected in SAX and ASCA data, but an upper limit was derived for the line flux. This was done by adding a gaussian feature to the fit. The centroid energy was allowed to vary in the 6.3–7.1 keV range. As the fit failed to find a statistically significant line, the 3σ upper limit of the line flux was estimated using the ‘error’ command of XSPEC. For the RXTE/PCA data, the same procedure detected the Fe K_α lines, with equivalent widths of ~ 80 –160 eV. The improvement in χ^2 was of the order 200 (for 37 degrees of freedom). No systematic errors were used in the fitting, but the Fe K_α line is statistically significant even with systematic errors. A systematic error of 1 % produces $\Delta\chi^2 \approx 60$ and a 2 % error $\Delta\chi^2 \approx 30$ for adding the Fe K_α line. The upper limit of the ASCA line flux is of the order 10 % of the detected RXTE/PCA flux. The parameters describing the final spectral fits are listed in Table 2 (continuum parameters) and 3 (line parameters).

To quantify the instrumental systematic effects on the iron line parameters, the RXTE calibration observations of the Crab were used. The standard products of Crab observations made near our observations (27.4, 9.5., 20.7, 12.9, 29.9, 12.10 and 13.10) were analyzed. The PCA 3–20 keV spectra were fitted with an absorbed powerlaw and a gaussian line. The line centroid energies were near 7 keV. The fluxes of the line and continuum were calculated in

a 1 keV band centered on the line centroid energy. The highest line to continuum ratio was 1.14 %. Typically the statistical error of the line to continuum ratio was a factor of 2–3, giving a 90 % upper limit of 3 % for the ratio. As the line to continuum flux ratios of the spectral fits of 4U 1543–624 vary between 3–7%, it can be concluded that the iron line has been detected. However, the line parameters of the RXTE fits listed in Table 3 are partially produced by instrumental uncertainties and therefore should be treated with some caution.

2.5. Temporal variability analysis

The ASCA/GIS and SAX/MECS lightcurves were extracted from cleaned event lists. RXTE (HEXTE and PCA) lightcurves were extracted from the event lists generated from the raw data. The HEXTE lightcurves were extracted in the 15–200 keV band. For PCA data, three bands were used, 2–5 keV (soft), 5–13 keV (medium) and 13–40 keV (hard) in the extraction process. No statistically significant periodic variations were detected in a Lomb–Scargle periodogram (Scargle 1982) made from the individual lightcurves. Absence of X-ray modulation suggests a relatively low inclination of the accretion disk.

Quasi-periodic oscillations (QPOs) were searched in the frequency range 10 kHz – 0.01 Hz (in the 3–10 keV band). Power spectra were extracted separately for each good time interval of all RXTE/PCA observations. After this, the power spectra were co-added to get a summed power spectrum. No statistically significant features (down to a few % rms amplitude) were seen in either the individual power spectra or the weighted mean.

To study the long-term variability, the lightcurve of the RXTE ASM (up to January 2002) was analyzed. No periodicities were detected in a Lomb–Scargle periodogram (Scargle 1982). In order to see if a trend is present in the ASM data, a linear model $F_{\text{ASM}} = A + Bt$ was fitted to the flux values. F_{ASM} is the observed ASM count rate (counts per second, 1 mCrab = 0.075 cps), A and B are the fit parameters and t is time in years from JD 2450000.5. The best fit values are $A = 3.269 \pm 0.0082$ and $B = -0.1735 \pm 0.0044$, but the improvement over a constant model in χ^2 is marginal (38887 to 37374).

To justify the fitting of a linear model, the literature was searched for older flux values of 4U 1543–624. MIR/Kvant observations (Emelyanov et al. 2000) on 30.1.1989 show a flux of 65 ± 11 mCrab ($1.71 \pm 0.29 \cdot 10^{-12} \text{ W m}^{-2}$) in the 2–30 keV band. An extrapolation of the linear fit predicts a flux 58.7 ± 0.1 mCrab for the Kvant observation, which is surprisingly close to the observed value. However, older observations show that the Kvant value is probably an isolated event and does not reflect an underlying trend. All the values listed below are absorbed fluxes in the 2–10 keV band, unless otherwise stated. The HEAO–1 (Wood et al. 1984) flux is $6.58 \pm 0.07 \cdot 10^{-13} \text{ W m}^{-2}$ (15.8.1977 to 15.2.1978), Ariel V (Warwick et al. 1981) $6.9 \pm 0.07 \cdot$

Table 2. The continuum parameters of the spectral fits with 90 % error estimates. Errors for the parameters derived from the fitted parameters have been calculated according to the propagation of errors. Line components are presented in Table 3. The values of luminosity (L) are unabsorbed 2–10 keV band values. For RXTE/PCA, the 2–3 keV part is based on extrapolation of the spectral fit. An assumed distance of 10 kpc has been used for the luminosity and BB radius estimates. The N_H values denoted with F have been held fixed (at $33 \cdot 10^{24} \text{ m}^{-2}$) during the fits. The Comptonization parameter is $\gamma_C = 4kT_C\tau_C^2/m_e c^2$. No systematic errors are included in the χ^2 values of the RXTE/PCA data.

Satellite	Date	L 10^{28} W	L_{BB}/L %	N_H 10^{24} m^{-2}	T_{BB} keV	R_{BB} km	T_C keV	τ_C	γ_C	χ_ν (dof)
ASCA	17.8.95	86	75	30_{-4}^{+3}	$1.55_{-0.03}^{+0.03}$	$3.21_{-0.11}^{+0.15}$	$0.54_{-0.03}^{+0.02}$	$33.0_{-2.8}^{+4.4}$	$4.6_{-0.8}^{+1.2}$	1.24 (394)
SAX	21.2.97	101	73	42_{-8}^{+6}	$1.677_{-0.017}^{+0.010}$	$2.99_{-0.09}^{+0.02}$	$0.70_{-0.03}^{+0.06}$	$22.0_{-0.9}^{+3.0}$	$2.7_{-0.3}^{+0.8}$	1.40 (527)
SAX	1.4.97	88	73	35_{-5}^{+7}	$1.575_{-0.008}^{+0.012}$	$3.14_{-0.09}^{+0.09}$	$0.57_{-0.03}^{+0.04}$	$29.7_{-3.6}^{+4.2}$	$3.9_{-1.0}^{+1.2}$	1.24 (528)
RXTE	5.5.97	123	38	33 F	$1.47_{-0.05}^{+0.02}$	$3.06_{-0.08}^{+0.08}$	$3.11_{-0.22}^{+0.20}$	$10.7_{-0.7}^{+0.9}$	$2.8_{-0.4}^{+0.5}$	0.79 (37)
RXTE	6.5.97	128	40	33 F	$1.48_{-0.03}^{+0.03}$	$3.18_{-0.13}^{+0.11}$	$3.02_{-0.36}^{+0.36}$	$10.9_{-1.3}^{+1.7}$	$2.8_{-0.7}^{+0.9}$	0.92 (37)
RXTE	7.5.97	123	42	33 F	$1.51_{-0.05}^{+0.08}$	$3.05_{-0.10}^{+0.08}$	$3.18_{-0.29}^{+0.29}$	$10.4_{-0.9}^{+1.3}$	$2.7_{-0.5}^{+0.7}$	1.16 (37)
RXTE	12.5.97	129	40	33 F	$1.48_{-0.03}^{+0.04}$	$3.14_{-0.09}^{+0.07}$	$3.04_{-0.16}^{+0.23}$	$11.1_{-1.2}^{+0.7}$	$2.9_{-0.6}^{+0.5}$	0.96 (37)
RXTE	14.5.97	130	37	33 F	$1.49_{-0.07}^{+0.02}$	$3.01_{-0.19}^{+0.19}$	$3.53_{-0.49}^{+0.52}$	$9.2_{-1.1}^{+1.6}$	$2.3_{-0.7}^{+0.9}$	0.74 (37)
RXTE	22.9.97	136	35	33 F	$1.48_{-0.05}^{+0.02}$	$3.03_{-0.17}^{+0.12}$	$2.94_{-0.24}^{+0.21}$	$11.1_{-1.0}^{+1.2}$	$2.8_{-0.5}^{+0.7}$	0.98 (37)
RXTE	13.10.97	127	38	33 F	$1.46_{-0.05}^{+0.04}$	$3.16_{-0.11}^{+0.11}$	$3.12_{-0.12}^{+0.30}$	$10.7_{-1.0}^{+1.1}$	$2.8_{-0.5}^{+0.6}$	0.71 (37)

$10^{-13} \text{ W m}^{-2}$, (15.10.1974 to 14.3.1980), varying between $3.0 - 12.0 \cdot 10^{-13} \text{ W m}^{-2}$, OSO-7 (Markert et al. 1979) $8.09 \pm 0.85 \cdot 10^{-13} \text{ W m}^{-2}$ (October 1971 to May 1973) and UHURU (Forman et al. 1978) $4.58 \pm 0.26 \cdot 10^{-13} \text{ W m}^{-2}$ (12.12.1970 to 18.3.1973). Einstein observations on 17.3.1979 (Christian & Swank 1997) give a flux of $\sim 7.0 \cdot 10^{-13} \text{ W m}^{-2}$ in the 0.5–20 keV band. The fluxes of the older surveys are clearly inconsistent with extrapolations of the linear model. The flux estimates of the 1970's missions have been derived from multiple scans, and more likely represent the average flux. Combining the results of the older missions with the ASM monitoring data indicates that the source variations are mainly irregular. The flux differences of the observations listed above, as well as the results of the pointed observations discussed below, indicate that flux variations by a factor of 2 may be seen on timescales of a few weeks.

3. Spectroscopic results

3.1. Continuum

The best-fit model has the same continuum components, an isothermal blackbody and a Comptonized component, as the fit to older EXOSAT data (Singh et al. 1994), and the BB and line parameters also have values consistent with the EXOSAT fit. The high S/N of the more modern instruments naturally gives much better constraints on the model parameters. The parameters of the Comptonized component are different (however, these were only weakly constrained for the EXOSAT fit, which has $kT_C > 4 \text{ keV}$ and $\tau_C < 4.8$). All continuum parameters are given in Table 2. The absorbing column depth is about one order of magnitude lower in the fits to the new data. In order to study this discrepancy, fits to archival EXOSAT data were made, with a column depth fixed to $N_H = 33 \cdot 10^{24} \text{ m}^{-2}$ (the value derived from fits to SAX and ASCA data). The values of the spectral parameters were similar to those derived from the ASCA and SAX fits, but the reduced

chi-squared of the fits was of the order $\chi_\nu = 1.4$. The old EXOSAT analysis is significantly better, $\chi_\nu = 1.16$ (Singh et al. 1994). The EXOSAT spectrum contains no information on fluxes below $\sim 1 \text{ keV}$ and the spectral resolution is rather modest at the low energy end. Therefore, it is possible that the absorbing column is not strongly constrained by the EXOSAT data.

A literature value of $N_H = 29.9 \pm 0.8 \cdot 10^{24} \text{ m}^{-2}$ can be found for Einstein data (Christian & Swank 1997). Analysis of the ASCA data with different absorption models gives column densities of $26\text{--}37 \cdot 10^{24} \text{ m}^{-2}$ (Juett et al. 2001). The galactic hydrogen column in the direction of 4U 1543–624 is $N_H \approx 30 \cdot 10^{24} \text{ m}^{-2}$ (Dickey & Lockman 1990). As the absorbing column is constrained better with observations covering lower energies, the ASCA, SAX and Einstein fits are most likely representing the correct value. However, the absorption may be influenced by matter local to 4U 1543–624 enriched in medium-Z elements (Juett et al. 2001).

The parameters of the Comptonized component and the overall luminosity vary significantly between observations. This can be interpreted as the system having two distinct states: when the system has higher luminosity it is referred to as being in the high state while when it has lower luminosity it is referred to as being in the low state. In the low state the Comptonized component is cooler ($kT \simeq 0.6 \text{ keV}$), with $\tau \simeq 30$. In the high state the Comptonized component is hotter ($kT \simeq 3 \text{ keV}$), with $\tau \simeq 10$. The luminosity (2–10 keV) is about 50 % higher in the high state, and the spectrum is significantly harder. A difference of this magnitude can not be explained by calibration errors. The BB is marginally hotter in the low state (1.6 vs. 1.5 keV). The RXTE observations show a high state spectrum. The ASCA observation and the SAX observation of 1.4.1997 show a low state spectrum. The SAX observation of 21.2.1997 shows a low state spectrum but the parameters are a little different from the two other low state spectra: the overall luminosity is higher,

Table 3. Detected Gaussian features. For the 6 keV feature, upper limits are given for the non-detections. Errors are 90 % confidence limits given by the XSPEC ‘error’ command. The RXTE fits were made with N_H fixed to $33 \cdot 10^{24} \text{ m}^{-2}$.

Dataset	Centroid keV	Flux $10^{-14} \text{ W m}^{-2}$	σ keV
ASCA 17.8.95	0.676 ± 0.016	$8.0_{-2.2}^{+4.6}$	$0.093_{-0.012}^{+0.005}$
SAX 21.2.97	0.67 ± 0.05	18_{-12}^{+49}	0.11 ± 0.04
SAX 1.4.97	0.67 ± 0.07	12_{-4}^{+6}	0.10 ± 0.03
ASCA 17.8.95	N/A	< 0.18	N/A
SAX 21.2.97	N/A	< 1.04	N/A
SAX 1.4.97	N/A	< 0.31	N/A
RXTE 5.5.97	$6.67_{-0.10}^{+0.08}$	$1.12_{-0.17}^{+0.41}$	$0.75_{-0.06}^{+0.15}$
RXTE 6.5.97	$6.65_{-0.17}^{+0.12}$	$0.94_{-0.30}^{+0.61}$	$0.63_{-0.25}^{+0.38}$
RXTE 7.5.97	$6.56_{-0.16}^{+0.12}$	$0.97_{-0.26}^{+0.41}$	$0.78_{-0.16}^{+0.22}$
RXTE 12.5.97	$6.61_{-0.14}^{+0.10}$	$0.84_{-0.26}^{+0.33}$	$0.68_{-0.24}^{+0.21}$
RXTE 14.5.97	$6.52_{-0.17}^{+0.20}$	$1.89_{-0.68}^{+0.48}$	$0.95_{-0.29}^{+0.21}$
RXTE 22.9.97	$6.46_{-0.15}^{+0.11}$	$1.43_{-0.36}^{+0.66}$	$0.76_{-0.18}^{+0.22}$
RXTE 13.10.97	$6.55_{-0.15}^{+0.12}$	$1.23_{-0.31}^{+0.49}$	$0.77_{-0.17}^{+0.20}$

the Comptonized component is slightly hotter and has a lower optical depth.

3.2. Narrow features

In the RXTE spectra the Fe K_α line is seen as a gaussian feature at $\approx 6.5 \text{ keV}$ with flux $\sim 10^{-14} \text{ W m}^{-2}$. Two flux values similar to this, $1.23 \cdot 10^{-14} \text{ W m}^{-2}$ (Singh et al. 1994) and $0.63 \cdot 10^{-14} \text{ W m}^{-2}$ (Gottwald et al. 1995) have been derived from the EXOSAT observation. The first value is from a dedicated study, the second one from the iron line catalogue, so the continuum model may be more refined in the first fit. A previous analysis of the ASCA data (Asai et al. 2000) has given line fluxes of 0.37 and $0.59 \cdot 10^{-14} \text{ W m}^{-2}$ for narrow and broad line models, respectively. However, the continuum model is fitted to data only in the band 4–10 keV, and the column density used is $N_H = 140 \cdot 10^{24} \text{ m}^{-2}$, considerably higher than the values derived from the same data. The possible differences in continuum slope and contribution of the iron K absorption edge at 7.1 keV to the spectrum are most likely responsible for the difference in the Fe K_α line parameters derived for the EXOSAT and ASCA observations.

Non-detection of the Fe K_α line in the ASCA and SAX/MECS spectra suggest variations of at least an order of magnitude in the line flux. The line is seen in observations from two different satellites (EXOSAT and RXTE). Therefore it is most probably safe to assume that the detection of the line is not caused by incorrect background subtraction.

Another gaussian feature is seen at $\approx 0.67 \text{ keV}$ in the SAX/LECS and ASCA/SIS spectra. All three observations have similar line parameters. The RXTE energy band does not cover the energy of this line. The feature may be a neon emission line. Another pos-

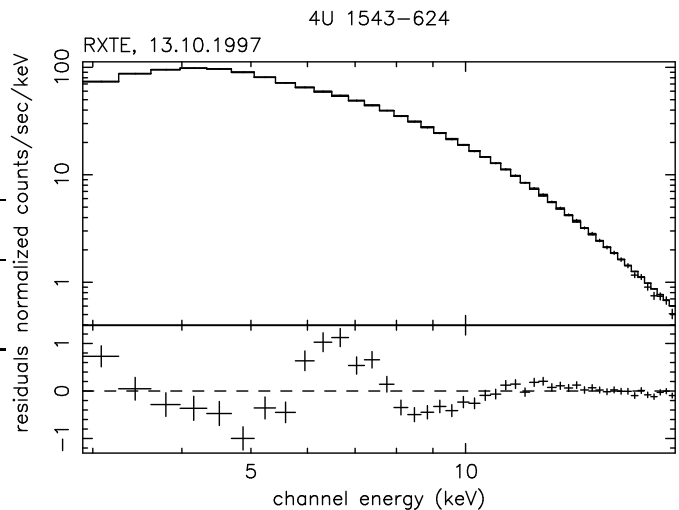


Fig. 2. A sample RXTE fit with BB and Comptonized component. The residuals indicate a line close to 6.5 keV.

sibility is enhanced absorption of Ne-enriched matter (Juett et al. 2001). The deeper absorption edge is seen as an artifact that is misinterpreted as a line.

4. Discussion

Potential black hole diagnostics include ultrasoft X-ray spectra, high-energy powerlaw ‘tails’, high-soft and low-hard spectral states and millisecond variability in the hard state (Tanaka & Lewin 1995). As 4U 1543–624 exhibits none of these features, it is assumed that the compact object is a neutron star. Asai et al. (2000) label 4U 1543–624 as an X-ray burster (which would confirm the neutron star nature of the compact object), but no reference is given.

4.1. The X-ray continuum

The isothermal blackbody originates from an optically thick boundary layer between the accretion disk and the neutron star surface (Sunyaev & Shakura 1986; see also Inogamov & Sunyaev 1999). The Comptonized component is produced by a corona of hot electrons upscattering soft photons from the disk. The energy of the Comptonized component is probably derived from the disk (see e.g. Church et al. (2002) and references therein).

The ratio of the boundary layer and inner disk luminosities should be close to unity if the neutron star is rotating slowly (Sunyaev & Shakura 1986). For faster rotators, the boundary layer should be less luminous, as the velocity of the accreted matter is closer to that of the neutron star surface. If the disk is truncated by the neutron star magnetosphere, its luminosity should be smaller (White et al. 1988). Stronger accretion flows should then push the inner disk closer to the compact object by decreasing the magnetosphere. The observed BB luminosity of 4U 1543–624 is about 3/4 of the total ($L_{BB}/L_{\text{comp}} \approx 3$) in the low state and slightly above 1/3

of the total ($L_{\text{BB}}/L_{\text{comp}} \approx 0.5$) in the high state. The ratio of the continuum component luminosities is relatively close to theoretical expectations for a slow rotator, suggesting the neutron star has not experienced spin-up to millisecond periods. Decreasing BB temperature in the high state reduces the BB luminosity slightly. It might be that the boundary layer is not radiating as a pure blackbody in the high state. Part of the luminosity difference could also be due to smaller inner disk radius, which would explain the higher disk (Comptonized component) luminosity. The blackbody fraction of the luminosity is clearly higher than in most LMXBs and in general the BB luminosity correlates strongly with total luminosity (Church et al. 2002; White et al. 1988).

4.2. Comptonizing corona

Observational evidence for Comptonizing coronae is quite convincing (White et al. 1988). No generally accepted model for the geometry (location, size and shape) of the Comptonizing coronae in LMXBs exists. A few geometries are discussed qualitatively below.

Should the corona be close to the boundary layer, the high optical depth of the Comptonized component would probably completely block any boundary layer emission. A clumpy Comptonizing corona could have high optical depth, and allow some boundary layer emission to shine through. Only a fraction of the boundary layer emission would then be intercepted by the corona. Reprocessed boundary layer photons would probably be seen as an additional X-ray continuum component. The higher temperature and lower optical depth of the clumps in the high state would be explained by evaporation of the outer parts of the clumps.

For a face-on system, a toroidal corona where the center is empty could produce the observed spectra. The accretion flow would be prevented from entering the central region by radiation pressure or the magnetic field of the neutron star. Near-Eddington accretion rates are needed to reach levels of radiation pressure that can influence the accretion flow. The X-ray flux of the source would imply a distance greater than 30 kpc for near-Eddington luminosities. Magnetic fields capable of controlling the corona far from the neutron star would also be able to control the bulk of the accretion flow near the surface. (The magnetic pressure scales as $P_B \propto B^2$ and for a dipole field $B^2 \propto r^{-6}$. For higher-order components, the scaling is steeper.) The absence of X-ray pulsations from such a system can be explained by geometrical effects. The influence of a magnetic field on the accretion flow could introduce a non-Maxwellian electron distribution, especially near the magnetic poles. This could in turn be seen as non-thermal hard X-ray emission from the neutron star surface, which is not observed. A corona controlled by the magnetic field could have a rather large vertical extent, as charged particles in a magnetic field can move rather freely along the field-lines. A mechanism that keeps the corona close to

the disk so that the input photons of the Comptonization are mainly from the soft disk radiation and not from the boundary layer is hard to find.

A ‘corona’ that is actually the upper part of the accretion disk, could also explain the observed properties. Such models usually have relatively low optical depths of the corona (Poutanen & Svensson 1996). The source of soft input photons is very close to the Comptonizing electrons. When viewed from the neutron star, the solid angle covered by the Comptonizing disk portion will be quite low, so the absence of processed boundary layer emission can be explained easily in this scenario. An increase in the accretion rate is likely to increase the vertical extent of the disk and the surface layer temperature, due to increased viscous heat release. An optically thick surface layer with a temperature in the keV range would practically prevent cooling of the bulk of the disk, resulting in mass loss, possibly through a disk wind. The response of the relative thicknesses of the layers to changes in accretion rates is unclear. Improved models for the interdependence of accretion rate and vertical disk structure are needed for a more quantitative discussion. This ‘flared-disk’ scenario seems to be an adequate explanation for the observed X-ray spectra.

4.3. Iron line

The flux of the Comptonized component and the flux of the 6 keV Fe K_α feature are both higher in the high state. In the low state, the line is undetected, with a flux lower by a factor of at least five to ten. This correlation suggests the components could be physically related. Potential sources for the Fe K_α feature are collisional excitation (Arnaud & Rothenflug 1985), radiative recombination (Arnaud & Raymond 1992), fluorescent emission and Compton reflection (Magdziarz & Zdziarski 1995).

The parameters of the Fe K_α line in the RXTE data are similar to those of the EXOSAT observation (Singh et al. 1994; Gottwald et al. 1995). The line energy is slightly above the 6.4 keV value, indicating ionization states up to Fe XXV (Nagase 1989). Collisional excitation would require temperatures of a few keV (Arnaud & Rothenflug 1985) to produce a line where the high ionization states dominate. These temperatures are similar to the observed temperature of the Comptonized component. The high line flux differences between the states (at least one order of magnitude) when the temperature drops by a factor of 4–5 is not straightforward to explain by pure collisional excitation. Photoionization may also influence the ionization state, as the gas emitting the Fe K_α line is irradiated by the accretion disk and the boundary layer. Radiative recombination of photoionized iron may be partially responsible for the line. More detailed modeling of the environment and better observational constraints on the Fe K_α line are needed before any firm conclusions regarding these mechanisms can be drawn.

If the line is produced by Compton reflection or fluorescence, the line flux should be proportional to the continuum providing the input energy or ‘seed photons’ for the line emission mechanism. For fluorescence, the seed photon energy is near 8 keV (iron absorption edge). The flux ratio of the Comptonized component in this band between the states is $\simeq 200$. As variations in the ionization state are not likely to change the fluorescent yield with a factor larger than 10 (Kallman 1995), fluorescence can not be ruled out by flux considerations. However, the large line width is hard to explain with fluorescence.

The Compton reflection seed photons have an energy very close to the line energy. In the low state, the flux of the Comptonized component (6–7 keV) is lower by a factor of $\simeq 20$. The ratio of the line and continuum (6–7 keV) fluxes in the high state is 0.04–0.1, suggesting a face-on disk (Magdziarz & Zdziarski 1995). If the ratio of Comptonized and reflected components remains constant during phase transitions, the line flux should be well below the detection limit in the low state. The fact that the BB component is not absorbed by the thick corona supports the face-on disk hypothesis. The above discussion shows that the mechanism producing the Fe K_α feature detected in the RXTE data can not be deduced from these observations alone.

4.4. Absorption and the 0.67 keV feature

The galactic coordinates of 4U 1543–624 are $\beta = -6.3$ and $\lambda = 321.8$. The total galactic hydrogen column density in this direction is $N_{\text{H}} \approx 30 \cdot 10^{24} \text{ m}^{-2}$ (Dickey & Lockman 1990). The X-ray spectral fits give similar values for the N_{H} , suggesting that 4U 1543–624 is at a distance greater than 10 kpc. Another possibility is that there is a local ISM component related to 4U 1543–624, increasing the absorption above the galactic value. The 0.67 keV feature could be an artifact of the local ISM (Juett et al. 2001), as interstellar absorption features complicate the analysis of the 0.67 keV feature. The neon absorption edge is very close to this, and the absorption of the ISM makes the continuum slope rather steep at these energies (see Fig. 1). These complications might also cause the changes in line/edge parameters when the continuum model is changed. The small differences in line parameters when comparing my results to those of Juett et al. (2001) are likely to be due to the different continuum model (powerlaw and BB with $kT \approx 0.4 \text{ keV}$). Juett et al. (2001) suggest observations with high spectral resolution near 0.67 keV to distinguish between an enhanced absorption edge and an emission line. Emission would more likely be related to only one of the continuum components, as absorption affects the total spectrum. As the ratio of continuum component fluxes varies considerably, observations in the high state with energy resolution comparable to ASCA or SAX would also help in finding the cause of the 0.67 keV feature. Unfortunately all observations with

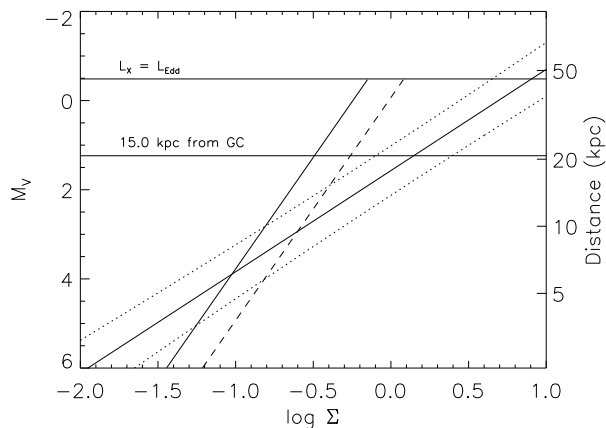


Fig. 3. Absolute visual magnitude M_V (left axis) and distance (right axis) of 4U 1543–624 against $\Sigma = P_{\text{hr}}^{2/3} (L_X/L_{\text{Edd}})^{1/2}$. The solid and dotted lines indicate the relation $M_V = 1.57 - 2.27 \log \Sigma$ with error estimates (Van Paradijs & McClintock 1994). An additional error term of 0.5 mag representing inclination variations is added to the original error estimates. To estimate the V magnitude, an intrinsic color $(B - V)_0 = -0.2$ is assumed. The column density of X-ray measurements has been used to estimate the extinction $A_B = 1.8$ and color excess $E_{B-V} = A_V/3 = 0.6$. The horizontal lines are upper limits for the distance assuming $L_X = L_{\text{Edd}}$ (for a $1.5 M_\odot$ NS and a He-rich donor) and 15 kpc distance from the Galactic Center. Note that the galactic latitude implies a distance of $z = r \sin \beta \approx 0.11r$ from the Galactic Plane. Constant-period lines represented by solid ($P = 36$ min) and dashed lines ($P = 80$ min) indicate the region of degenerate donors. Systems with periods below 36 min and observable accretion rates are most likely produced by tidal capture. It seems possible that the system has a very short period.

instruments capable of detecting the the 0.67 keV feature have been made in the low state.

The N_{H} from the X-ray spectral fits presented above should give a visual extinction of $A_V \approx 1.8$ (Predehl & Schmitt 1995; Bohlin et al. 1978). The optical counterpart has been identified as a $B \approx 20$ magnitude star (McClintock et al. 1978). The LMXB optical emission is usually dominated by the accretion disk. The intrinsic color indices are in the range $(B - V)_0 = [-0.5, 0.5]$, the average being around -0.2 (Van Paradijs & McClintock 1995). The known absolute visual magnitudes are between $M_V = [-5, 6]$ (Van Paradijs & McClintock 1994), and the weaker sources with $M_B < 0$ are generally X-ray bursters. After correcting for absorption, the ratio of X-ray (2–10 keV) to optical luminosity is $L_X/L_{\text{opt}} \approx 480$, a typical LMXB value (Van Paradijs & McClintock 1995).

The galactic coordinates of 4U 1543–624 ($\beta = -6.3$ and $\lambda = 321.8$) imply a minimum distance between the

source and Galactic Center of ≈ 5.6 kpc (assuming a distance of 8.6 kpc for the Galactic Center). Therefore 4U 1543–624 is probably a member of the disk population, and the common literature value of distance 10 kpc, more representative for the bulge population, should be regarded as an order-of-magnitude estimate. Using the empirical relation between optical and X-ray fluxes and the period (Van Paradijs & McClintock 1994), it can be concluded that the system may have a degenerate donor (Fig. 3), and the distance is likely to be in the range 3–20 kpc.

5. Conclusions

Archival X-ray observations of 4U 1543–624 have been analyzed. The X-ray continuum can be fitted with a two-component model consisting of an isothermal blackbody and a Comptonized component. Two different X-ray states are seen. In the high state, the luminosity comes mainly from the Comptonized component and the spectrum is harder. The low state spectrum is dominated by the BB, but the Comptonized component is also important at energies below 2 keV. Two gaussian features at 6.5 keV (the Fe K_{α} line) and 0.67 keV are detected. The Fe K_{α} line is seen only in the high state, and it has at least one order of magnitude lower flux in the low state. A two-layer disk, with the lower and cooler layer providing the input photons to be upscattered by the hotter surface layer, provides a qualitative explanation for the X-ray continuum and state transitions.

The BB component of the X-ray spectrum can be taken as weak evidence of a neutron star. It is probably safe to assume that the BB comes from a boundary layer between the neutron star surface and the inner disk, and the Comptonized component is from a hot disk corona. The ratio of the continuum component luminosities is close to unity. This is in good accordance with the theoretical expectation for a slowly rotating neutron star (Sunyaev & Shakura 1986). Most LMXBs have lower BB luminosities (White et al. 1988). A rapidly rotating neutron star or non-thermal emission from the boundary layer have been suggested to explain this discrepancy. In LMXBs with detected BB emission, the BB luminosity correlates strongly with total luminosity. The BB luminosity of 4U 1543–624 decreases slightly when the total luminosity increases significantly. The changes seen in continuum spectrum and its variations, which are opposite to observations of other LMXBs, can be explained if 4U 1543–624 has a boundary layer with a spectrum close to BB and a slowly rotating neutron star ($P \gg$ ms).

Angular momentum of the accreted matter tends to spin up the neutron stars. An equilibrium between angular momentum gain from the accretion flow and losses due to gravitational radiation is reached at periods of the order one millisecond. For typical LMXB accretion rates the equilibrium is reached in a time of the order 10^7 years (Rappaport et al. 1983). The observations suggest that 4U 1543–624 has gained less angular momentum. It has either been accreting for a shorter time than a typ-

ical LMXB, or the accretion rate is significantly smaller. Monitoring observations with sufficient energy resolution to estimate the continuum components would be especially useful. Such observations have the best possibility of observing the system in a wide range of states.

The gaussian feature seen in the RXTE high state spectra near 6.5 keV is interpreted as the Fe K_{α} line. The line parameters are partially produced by instrumental effects, and should be treated with some caution. As the line is absent in the low state, with an upper flux limit one order of magnitude lower than the observed RXTE flux, the line is probably related to the Comptonized component. The line is broad and the centroid energy is above the neutral iron value, suggesting it might originate from ionized gas. Possible mechanisms producing this line are radiative recombination (Arnaud & Raymond 1992), collisional excitation (Arnaud & Rothenflug 1985) and Compton reflection (Magdziarz & Zdziarski 1995). The line width implies fluorescence is less likely to be responsible for the line. High S/N low-state spectra are needed to provide better constraints on the line formation. If the low-state Fe K_{α} fluxes are close to the upper limit derived from ASCA data, more detailed modeling than presented here is needed. On the other hand, very low line fluxes would favour the Compton reflection mechanism. The two-layer disk model providing the best qualitative explanation for the Comptonized spectrum could easily produce such a reflected component.

The 0.67 keV feature has been detected previously in ASCA data (Juett et al. 2001). It also detected in SAX data, and the parameters do not change significantly, when a different continuum model is used. This analysis confirms the detection of the 0.67 keV feature. The feature is either a neon absorption edge, made stronger by enhanced neon abundance (Juett et al. 2001), or an emission line. Juett et al. (2001) suggest observations with very high spectral resolution to distinguish between the two mechanisms producing the feature. The detected state transitions show that the distinction could also be made by comparing medium-resolution observations in the two states. If the feature strength changes with state, the line interpretation is more likely. Changes in the continuum component physically related to the line are likely to produce changes in the line parameters. If the equivalent width of the feature remains unchanged during state transitions, it is more likely to be the absorption edge.

Optical spectroscopy of the system would allow determining the abundances of the inflowing matter. The equivalent widths of the lines near 460 nm He II, C III, N III and $H\beta$ could provide the needed abundance diagnostics. A short-period system with a degenerate donor would have stronger He and possibly CNO lines and weaker $H\beta$ line than a system with a main sequence donor.

Acknowledgements. I am grateful to Pasi Hakala, Panu Muhli and Osmi Vilhu for useful discussions, and to Diana Hannikainen for both useful discussions and checking the English of the manuscript. I thank the anonymous referee

for his/her useful comments. This research has made use of NASA's Astrophysics Data System (ADS) Bibliographic Services and data obtained from the High Energy Astrophysics Science Archive Research Center (HEASARC), provided by NASA's Goddard Space Flight Center, and the SIMBAD database, operated at CDS, Strasbourg, France. Financial support of Academy of Finland and the National Technology Agency TEKES is acknowledged.

References

- Apparao K.M.V., Bradt H.V., Dower R.G. et al., 1978, *Nature* 271, 225
- Arnaud K.A., 1996, In 'Astronomical Data Analysis Software Systems V', ASP Conference Series 101, eds. Jacoby G. & Barnes J., San Fransisco: ASP, 17
- Arnaud M. & Raymond J., 1992, *ApJ* 392, 394
- Arnaud M. & Rothenflug R., 1985, *A&AS* 60, 425
- Asai K., Dotani T., Nagase F. & Mitsuda K., 2000, *ApJS* 131, 571
- Boella G., Chiappetti L., Conti G. et al, 1997, *A&AS* 122, 327
- Bohlin R.C., Savage B.D. & Drake J.H., 1978, *ApJ* 224, 132
- Bradt H.V., Rothschild R.E. & Swank J.H., 1993, *A&AS* 97, 355
- Christian D.J. & Swank J.H, 1997, *ApJS* 109, 177
- Church M.J., Inogamov N.A. & Balucinska-Church M., 2002, *A&A* 390, 139
- Dickey J.M. & Lockman F.J 1990, *ARA&A* 28, 215
- Emelyanov A.N., Aleksandovich N.L. & Sunyaev R.A., 2000, *Astro. Lett.* 26, 297
- Fiore F., Guainazzi M. & Grandi P., 1999 'Cookbook for BeppoSAX NFI Spectral Analysis', available by ftp from [legacy.gsfc.nasa.gov/sax/doc/software_docs/saxabc_v1.2.ps](ftp://legacy.gsfc.nasa.gov/sax/doc/software_docs/saxabc_v1.2.ps)
- Forman W., Jones C., Cominsky L. et al., 1978, *ApJS* 38, 357
- Frontera F., Costa E., dal Fiume D. et al., 1997, *A&AS* 122, 357
- Gottwald M., Parmar A.N., Reynolds A.P. et al., 1995, *A&AS* 109, 9
- Inogamov N.A. & Sunyaev R.A., 1999, *Astro. Lett.* 25, 269
- Jahoda K., Swank J.H., Giles A.B. et al., 1996, *Proc SPIE* 2808, 59
- Juett A.M., Psaltis D. & Chakrabarty D., 2001, *ApJL* 560, 59
- Kallman T.R., 1995, *ApJ* 455, 603
- Levine A.M., Bradt H., Cui W. et al., 1996, *ApJL* 469, 33
- Magdziarz P. & Zdziarski A., 1995, *MNRAS* 273, 837
- Makishima K., Maejima Y., Mitsuda K. et al., 1986, *ApJ* 308, 635
- Manzo G., Giarrusso S., Santangelo A. et al., 1997, *A&AS* 122, 341
- Markert T.H., Laird F.N., Clark G.W. et al., 1979, *ApJS* 39, 573
- McClintock J.E., Canizares C.R., Hiltner W.A. & Petro L., 1978, *IAUC* 3251
- Nagase F., 1989, *PASJ* 41, 1
- Parmar A.N., Martin D.D.E., Bavdaz M. et al., 1997, *A&AS* 122, 309
- Poutanen J. & Svensson R., 1996, *ApJ* 470, 249
- Predehl P. & Schmitt J.H.M.M., 1995, *A&A* 293, 889
- Rappaport S., Verbunt F. & Joss P.C., 1983, *ApJ* 275, 713
- Scargle J.D., 1982, *ApJ* 263, 835
- Singh K.P., Apparao K.M.V. & Kraft R.P., 1994, *ApJ* 421, 753
- Sunyaev R.A. & Shakura N.I., 1986, *Soviet Astron. Lett.* 12, 117
- Sunyaev R. & Titarchuk L., 1980, *A&A* 86, 121
- Tanaka Y., Inoue H. & Holt S.S., 1994, *PASJ* 46, L37
- Tanaka Y. & Lewin W.H.G., 1995, In 'X-ray binaries', eds. Lewin W.H.G., van Paradijs J. & van den Heuvel E.P.J., Cambridge University press
- Titarchuk L., 1994, *ApJ* 434, 313.
- Van Paradijs J. & McClintock J.E., 1994, *A&A* 290, 133
- Van Paradijs J. & McClintock J.E., 1995, In 'X-ray binaries', eds. Lewin W.H.G., van Paradijs J. & van den Heuvel E.P.J., Cambridge University press
- Warwick K.S., Marshall N., Fraser G.W. et al., 1981, *MNRAS* 197, 865
- White N.E., Stella L. & Parmar A.N., 1988, *ApJ* 324, 363
- Wood K.S., Meekins J.F., Yentis D.J. et al., 1984, *ApJS* 56, 507